Fundamental Research 3 (2023) 611–617

Contents lists available at ScienceDirect

Fundamental Research

journal homepage: http://www.keaipublishing.com/en/journals/fundamental-research/

Article

Alkyl side chain engineering enables high performance as-cast organic solar cells of over 17% efficiency

Xiang Xu[a], Yazhou Qi[a], Xiaoyan Luo[a], Xinxin Xia[b], Xinhui Lu[b], Jun Yuan[a], Yonghua Zhou[a], Yingping Zou[a,*]

[a] State Key Laboratory of Powder Metallurgy, College of Chemistry and Chemical Engineering, Central South University, Changsha 410083, China
[b] Department of Physics, The Chinese University of Hong Kong, New Territories, Hong Kong 999077, China

ARTICLE INFO

Article history:
Received 18 November 2021
Received in revised form 16 December 2021
Accepted 14 January 2022
Available online 11 February 2022

Keywords:
Organic solar cells
Alkyl side chains
As-cast
Green solvent
Stability

ABSTRACT

Achieving high-performance as-cast OSCs is crucial for industrialization in the future, owing to the advantages of better stability, environmental-friendly, and decreasing production cost. In this regard, we synthesized an A-DA′D-A type acceptor, Y6-eC6-BO, by shortening the straight alkyl side-chains on the thiophene position from C_{11} to C_6 as well as lengthening the branched alkyl side-chains on the pyrrole position of Y6 to achieve a stronger crystallization and better miscibility than Y6. As a result, the corresponding chloroform-processed as-cast PM6:Y6-eC6-BO OSC showed a high PCE of 17.33%, which was one of the highest efficiencies of as-cast OSCs. And the as-cast PM6:Y6-eC6-BO OSCs processed from *o*-xylene displayed a PCE of 16.38%, as far as we know, this is among the highest efficiencies of non-halogenated-solvent processed as-cast OSCs. These results demonstrated tailoring the alkyl side-chain of NFAs is a feasible and simple approach to achieve high performance as-cast OSCs and provides guideline in molecular design in the future.

1. Introduction

In recent years, organic solar cells (OSCs) have become one of important photovoltaic technology owing to solution processing, flexibility, semi-transparent, non-toxicity, and so on [1–3]. The increasing novel active layer and interfacial materials strongly boosted the progress of OSCs, among them, the first reported BZIC with A-DA′D-A structure has opened the new door to develop high performance non-fullerene acceptor material systems [4]. For example, the A-DA′D-A molecule Y6, in which the backbone adopts "Y"-shape geometry, has pushed the power conversion efficiency (PCE) of OSCs over 15% [5,6]. Hereafter, a series of modified acceptors with A-DA′D-A structure are developed, eventually, the efficiencies of them have reached over 18% up to now [7–11].

Aside from the design of novel conjugated materials, some device optimization methods play a vital role in tuning the phase separation of bulk-heterojunction (BHJ), thus resulting in the optimized performance of OSCs, such as thermal annealing (TA) [12], additives [13,14] and solvent annealing [15,16]. In particular, haloid 1,8-diiodooctane (DIO) and 1-chloronaphthalene (CN) additives even become one of the prerequisites for obtaining high performance OSCs [17]. However, these methods not only exhibit poor compatibility with mass production in the future, but also generally bring a lot of new problems, such as stability, environmental friendliness, production costs [18–20]. In general, high boiling point solvent additives are difficult to be removed completely and can also easily form undesirable metastable morphology. For instance, residual DIO will release iodide radicals under light and these radicals may react with active layer materials, leading to degradation [21]. Therefore, developing high-performance as-cast OSCs is urgent to meet the demand of large-scale production in the future [22–24]. Recently, Lin *et al.* have synthesized a novel non-fullerene acceptor Y6Se by substituting selenium for sulfur atom of benzothiadiazole (BT) in Y6. As a result, as-cast D18:Y6Se OSC displayed a higher PCE of 17.7% than D18:Y6 [25]. Furthermore, they have introduced an asymmetric polarizable alkoxy side-chain on the pyrrole position of Y6, resulting in the synthesis of Y6-4O. Y6-4O exhibited a higher dielectric constant and better solubility than Y6. As a consequence, the as-cast PM6:Y6-4O OSCs processed from non-halogen solvent showed a PCE of 15.2% [26].

However, PM6:Y6-based OSCs only could achieve higher PCE with CN additive and thermal annealing relative to as-cast counterpart [5]. In this work, we aim to achieve high-performance as-cast OSCs by tailoring the alkyl side chains on Y6 (2,2′-((2Z,2′Z)-((12,13-bis(2-ethylhexyl)-3,9-diundecyl-12,13-dihydro- [1,2,5]thiadiazolo [3,4-e]thieno [2″,3″:4′,5′]thieno [2′,3′:4,5]pyrrolo [3,2-g]thieno [2′,3′:4,5]-thieno [3,2-b]indole-2,10-diyl)bis(methanylylidene))bis(5,6-

* Corresponding author.
E-mail address: yingpingzou@csu.edu.cn (Y. Zou).

https://doi.org/10.1016/j.fmre.2022.01.025

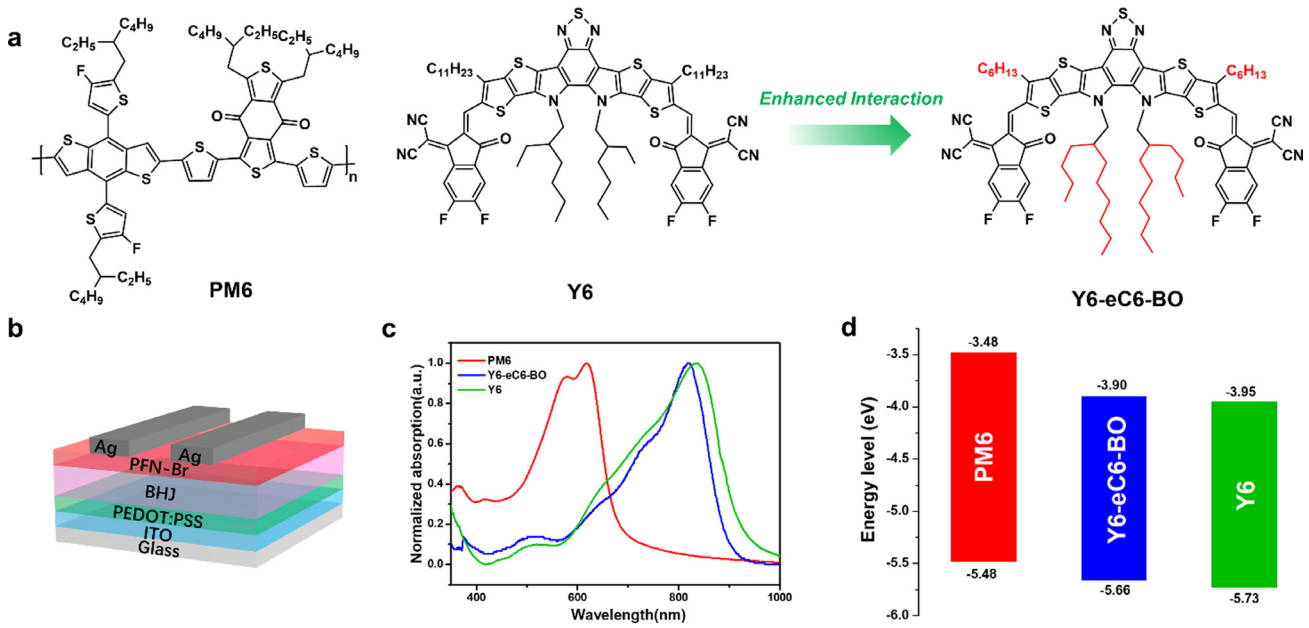

Fig. 1. Molecular structures, properties, and device structure. (a) Chemical structures of the PM6, Y6, and Y6-eC6-BO. (b) Device structure with a conventional configuration was used in this work. (c) UV-vis absorption spectra of the donor and acceptor materials in film state. (d) Energy level alignment of the donor and acceptor materials.

difluoro-3-oxo-2,3-dihydro-1H-indene-2,1-diylidene))dimalononitrile) to simultaneously improve crystallization and miscibility. Thereby, a new alkyl-modified non-fullerene acceptor, Y6-eC6-BO (shown in Fig. 1), was synthesized. Compared to Y6, Y6-eC6-BO exhibits better miscibility with PM6 (poly [1-(5-(4,8-bis(5-(2-ethylhexyl)-4-fluorothiophen-2-yl)-6-methylbenzo [1,2-b:4,5-b]dithiophen-2-yl)thiophen-2-yl)-5,7-bis(2-ethylhexyl)-3-(5-methylthiophen-2-yl)-4H,8H-benzo [1,2-c:4,5-c]dithiophene-4,8-dione])), which is beneficial for forming interpenetrating network architecture without the aid of additive and thermal annealing. As a result, as-cast PM6:Y6-eC6-BO OSCs exhibit a high PCE of 17.33%, which is one of the highest efficiencies of as-cast OSCs to date. In addition, Y6-eC6-BO has a great potential in green solvent processing that meets the demand for environmental protection. In this regard, as-cast PM6:Y6-eC6-BO OSCs processed from non-halogen ortho-xylene (*o*-XY) display a PCE of 16.38%, which is listed among the highest efficiencies of non-halogenated-solvent processed as-cast OSCs so far. Moreover, the as-cast OSCs possess better stability than the CN-additive-treated devices. This work demonstrates that the high-performance as-cast OSCs could be achieved by a simple and feasible alkyl-modified strategy.

2. Results and discussion

The chemical structures of the active layer materials used in this work are shown in Fig. 1a. Compared to Y6, Y6-eC6-BO was modified by shortening the straight alkyl side-chains on the thiophene position from C_{11} to C_6 as well as lengthening the branched alkyl side-chains on the pyrrole position. The synthesis of Y6-eC6-BO is shown in Section 1.2 in Supplementary Materials. The absorption spectra of PM6, Y6, and Y6-eC6-BO films are depicted in Fig. 1c, and the absorption spectrum of Y6-eC6-BO solution in $CHCl_3$ as well as PM6:Y6 and PM6:Y6-eC6-BO blend films are shown in Fig. S3. The absorption data of Y6-eC6-BO are summarized in Table 1. Both Y6 and Y6-eC6-BO had a complementary absorption with PM6, however, Y6-eC6-BO film displayed a blue-shifted absorption of about 17 nm in contrast with Y6. Previous studies demonstrated that the modification of alkyl side-chain leads to different molecular packings, thus, both absorption and electronic energy level properties of the acceptor materials will be changed [7,27].

Table 1
Absorption properties and energy levels of Y6-eC6-BO.

Acceptor	λ_{max}^{sol} (nm)	λ_{max}^{film} (nm)	λ_{onset}^{film} (nm)	E_g^{opt} (eV)	E_{HOMO} (eV)	E_{LUMO} (eV)
Y6-eC6-BO	733	820	911	1.36	-5.66	-3.90

The electronic energy level measurements of PM6, Y6, and Y6-eC6-BO were performed by cyclic voltammetry (CV) method, and the extracted highest occupied molecular orbital (HOMO) and lowest unoccupied molecular orbital (LUMO) energy levels were depicted in Fig. 1d and also listed in Table 1 (the cyclic voltammograms are shown in Fig. S4). Y6-eC6-BO possesses a shallower LUMO and HOMO than Y6, which is beneficial for improving the open-circuit voltage (V_{oc}). And a smaller ΔE_{LUMO} offset between PM6 and Y6-eC6-BO still provided enough driving force for exciton dissociation.

To investigate the photovoltaic properties of the studied devices under one sun illumination, the device structure that is used in this work is glass/ indium tin oxide (ITO)/poly(3,4-ethylenedioxythiophene):poly(styrenesulfonate) (PEDOT:PSS)/bulk-heterojunction (BHJ)/PFN-Br/Ag as shown in Fig. 1b. By blending with PM6, the as-cast (hereafter simplified as AC) Y6-based OSCs only obtained a poor performance relative to the optimized devices. The current density-voltage (*J-V*) curves are plotted in Fig. 2a, and corresponding photovoltaic parameters are summarized in Table 2 (the detailed data are shown in Table S1). The as-cast PM6:Y6 OSCs only showed a PCE of 13.30% with V_{oc} of 0.825 V, J_{sc} of 24.49 mA/cm^2 and FF of 65.81%. After being treated with CN and thermal annealing, the optimal PM6:Y6 device gave a better photovoltaic performance with a PCE of 16.08% (V_{oc} of 0.834 V, J_{sc} of 26.45 mA/cm^2 and FF of 72.85%), which is consistent with the reported performance. By contrast, the as-cast PM6:Y6-eC6-BO device exhibited the highest PCE of 17.33% with V_{oc} of 0.846 V, J_{sc} of 26.44 mA/cm^2 and FF of 77.42%. To our best knowledge, this is one of the highest efficiencies of as-cast OSCs until now. While the optimized (hereafter simplified as OP) PM6:Y6-eC6-BO device displayed a slight poor performance. And the higher V_{oc} of the PM6:Y6-eC6-BO device than the Y6-based devices could be ascribed to the shallow LUMO energy level of Y6-eC6-BO

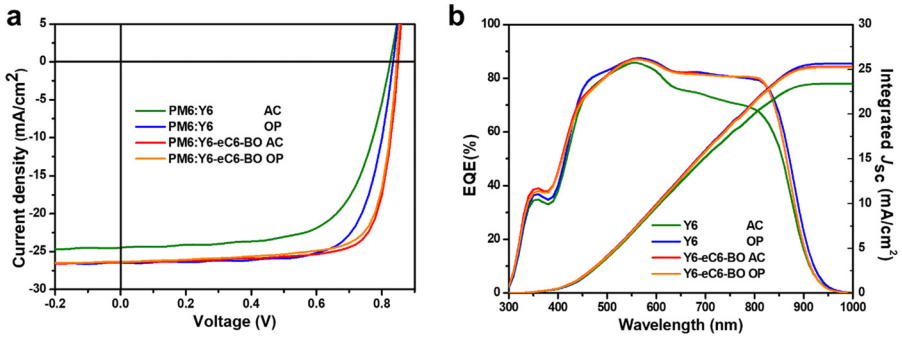

Fig. 2. Photovoltaic characteristics of the OSCs. (a) The *J-V* curves of as-cast (AC) or optimized (OP) PM6:Y6 and PM6:Y6-eC6-BO devices under 1sun illumination. (b) EQE curves and corresponding integrated J_{sc} of as-cast or optimized PM6:Y6 and PM6:Y6-eC6-BO devices.

Table 2
Photovoltaic parameters of the OSCs with or without any treatment under 1 sun illumination.

BHJ	condition	V_{oc} (V)	J_{sc} (mA cm^{-2})	FF (%)	PCE (%)	$J_{sc\text{-}EQE}$ (mA cm^{-2})
PM6:Y6 [a)]	As-cast	0.825	24.49	65.81	13.30 (13.04±0.31)	23.37
PM6:Y6 [b)]	Optimized	0.834	26.45	72.85	16.08 (15.80±0.28)	25.63
PM6:Y6-eC6-BO [a)]	As-cast	0.846	26.44	77.42	17.33 (17.07±0.25)	25.30
PM6:Y6-eC6-BO [b)]	Optimized	0.841	26.32	75.72	16.76 (16.55±0.23)	25.21

a) The OSC devices are processed without any treatment.
b) The devices are optimized by 0.5% CN (volume ratio) and 100 °C thermal annealing of 10 min. The data shown in brackets are averaged from over 10 devices and $J_{sc\text{-}EQE}$ is the photocurrent integrated from the EQE spectrum.

acceptor as mentioned above. Furthermore, the external quantum efficiency (EQE) and corresponding integrated J_{sc} curves are plotted in Fig. 2b (the J_{sc} difference derived from sun simulator and EQE spectra is within an error of 5%). The as-cast PM6:Y6 device obtained a poor integrated J_{sc} from EQE spectrum in all studied devices, which was due to the sharp decrease of quantum response efficiency from the region of 550 to 850 nm. Also, the EQE response edge of the OSC based on PM6:Y6-eC6-BO was slightly blue-shifted than the Y6-based devices that were consistent with the blue-shifted absorption spectrum as well.

To gain more insight into the impact of microstructure on the properties of the studied OSCs, morphology investigations were performed by transmission electron microscope (TEM), atomic force microscope (AFM), and grazing-incidence wide-angle X-ray scattering (GIWAXS) techniques [28]. The TEM and AFM height, as well as phase images, are displayed in Fig. 3. In the AFM height and phase images, the bright and brown phases can be regarded to the donor- and acceptor-rich domains, respectively [29,30]. This is because the polymer donor will form a fibrous structure, while the molecular acceptor is scattered around. Thus, we can get very visualized information about phase separation. As shown in Fig. 3e-l, the as-cast PM6:Y6 film displayed a quite severe aggregation behavior according to the large and coterminous donor as well as acceptor domains. After the treatments of CN additive and thermal annealing, this worsening case was mitigated. And the obvious fiber-like structure with better phase separation was observed by TEM images. In addition, the as-cast PM6:Y6-eC6-BO film showed a homogeneous and interpenetrating nano-phase separation, and the root-mean-square (RMS) roughness was only 1.04 nm. While the PM6: Y6-eC6-BO film with the treatments of CN additive and thermal annealing (TA) exhibited an increased aggregation behavior of the acceptor which will result in reduced D/A interfaces and the fiber-like structure became slightly unclear, the RMS roughness was increased to 2.23 nm as well.

The GIWAXS scattering patterns and profiles of the studied blend films are plotted in Fig. 4a-b (the corresponding 2D patterns and 1D profiles of pristine PM6, Y6, and Y6-eC6-BO films are summarized in Fig. S5), respectively. We can observe that the pristine Y6-eC6-BO film had strong (010) and (*h*00) scattering peaks, whereas only an obvious (010) peak belonged to the Y6 film. And the coherence lengths (CL=2πk/fwhm, where K is a shape factor of 0.9, fwhm is full width at half maximum of peak) of common (010) peak of Y6 and Y6-eC6-BO were 1.93 nm and 2.37 nm, respectively. In general, a larger CL is associated with strong crystalline capacity. By blending with PM6, both PM6:Y6 films showed a strong (010) reflection of the π-π stacking peak at 17.6 nm^{-1} in the out-of-plane (OOP) direction, whereas CL was increased from 1.98 nm to 2.56 nm after optimization, indicating a stronger crystallization and better face-on orientation of Y6. In addition, the (*h*00) reflection of the lamella stacking peak at 3 nm^{-1} showed an obvious enhancement as well. The as-cast PM6:Y6-eC6-BO film displayed a similar π-π stacking peak at 17.6 nm^{-1} in the out-of-plane (OOP) direction, with a suitable CL of 2.85 nm which could be attributed to a stronger crystallization of Y6-eC6-BO than Y6. The treated PM6:Y6-eC6-BO film exhibited a closer π-π stacking owing to the (010) peak located at 18.1 nm^{-1}, and the calculated CL was extracted to be an over-large 4.2 nm. In the IP direction, multiple diffraction peaks revealed that the crystallization of Y6-eC6-BO was strongly improved. However, the excessive crystallization of Y6-eC6-BO will result in over-large phase separation that is demonstrated by the AFM image. These results uncovered the as-cast Y6-eC6-BO not only had excellent miscibility with PM6 and the inherent strong crystallization but also achieved a balance between miscibility and crystallization.

To further study the phase separation properties of PM6: Y6 and PM6: Y6-eC6-BO blends, the Flory-Huggins interaction parameters ($\chi_{Donor,\ Acceptor} \propto (\sqrt{\gamma_{Donor}} - \sqrt{\gamma_{NFA}})^2$) were calculated from contact angle measurements [31] (the original contact angle images are shown in Fig. S6, and the corresponding surface energies are calculated by Owens equation [32]) and summarized in Table 3. Concerning the high-boiling CN additive still maintained in BHJ, thus we fabricated the PM6, Y6, and Y6-eC6-BO films with or without 0.5% CN treatment. It was evident that all the pristine films had higher surface energy than the CN-treated films, this could be ascribed to the inherent hydrophobic property of CN. Among them, Y6 film exhibited a sharp decrease from 37.16 mN/m to 26.09 mN/m after being treated with CN, while the Y6-eC6-BO film showed a slight change in surface energy after optimization. The resulting Flory-Huggins interaction parameters were calculated based on the above-mentioned equation. We could find that the as-cast PM6:Y6 blend afforded the highest χ of 1.28, which was in accordance with the above morphology images. Also, the χ of optimized PM6:Y6 blend was

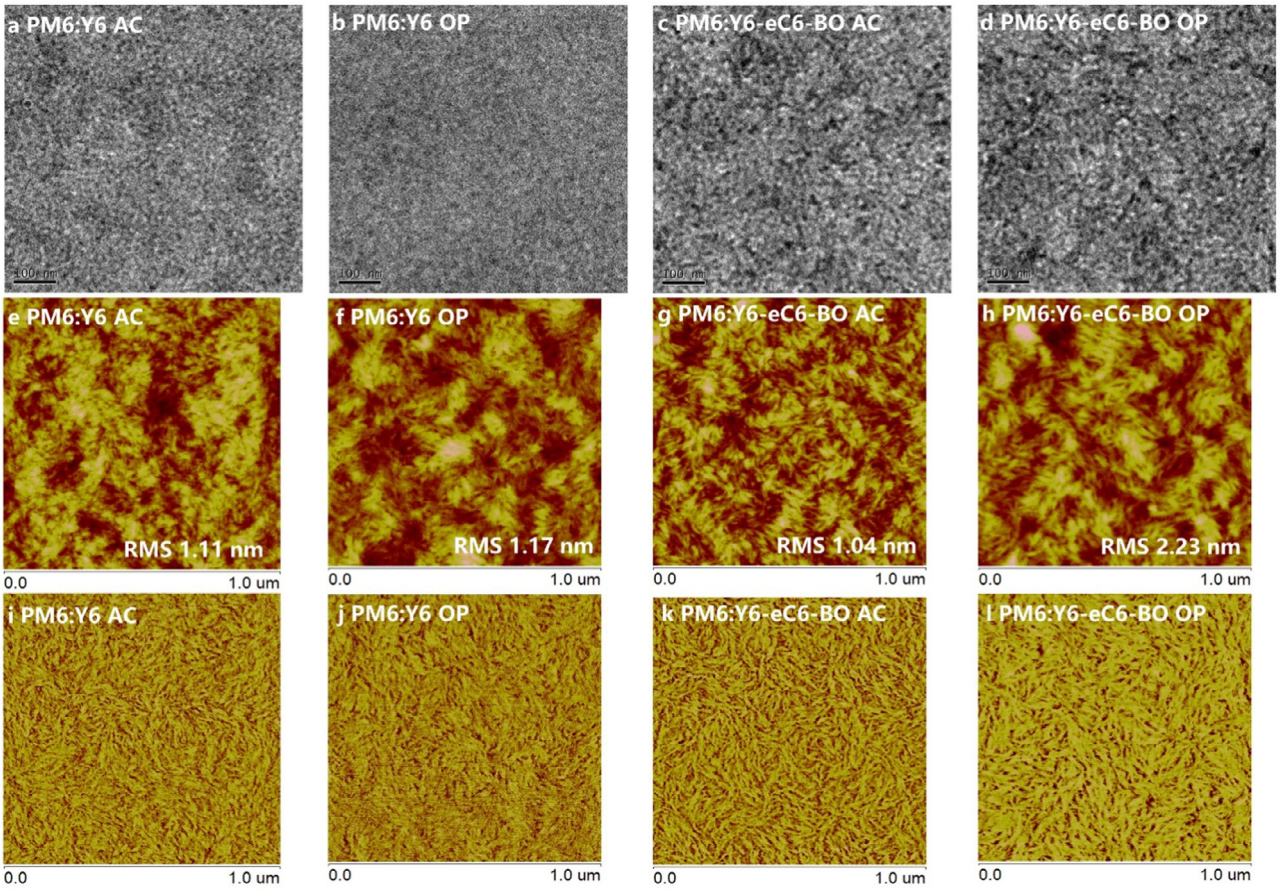

Fig. 3. Morphology characteristics of the films. (a-d) TEM and (e-h) 1μm × 1μm scaled AFM height and (i-l) phase images of the as-cast (AC) PM6:Y6 film, optimized (OP) PM6:Y6 film, as-cast (AC) PM6:Y6-eC6-BO film and optimized (OP) PM6:Y6-eC6-BO film, respectively.

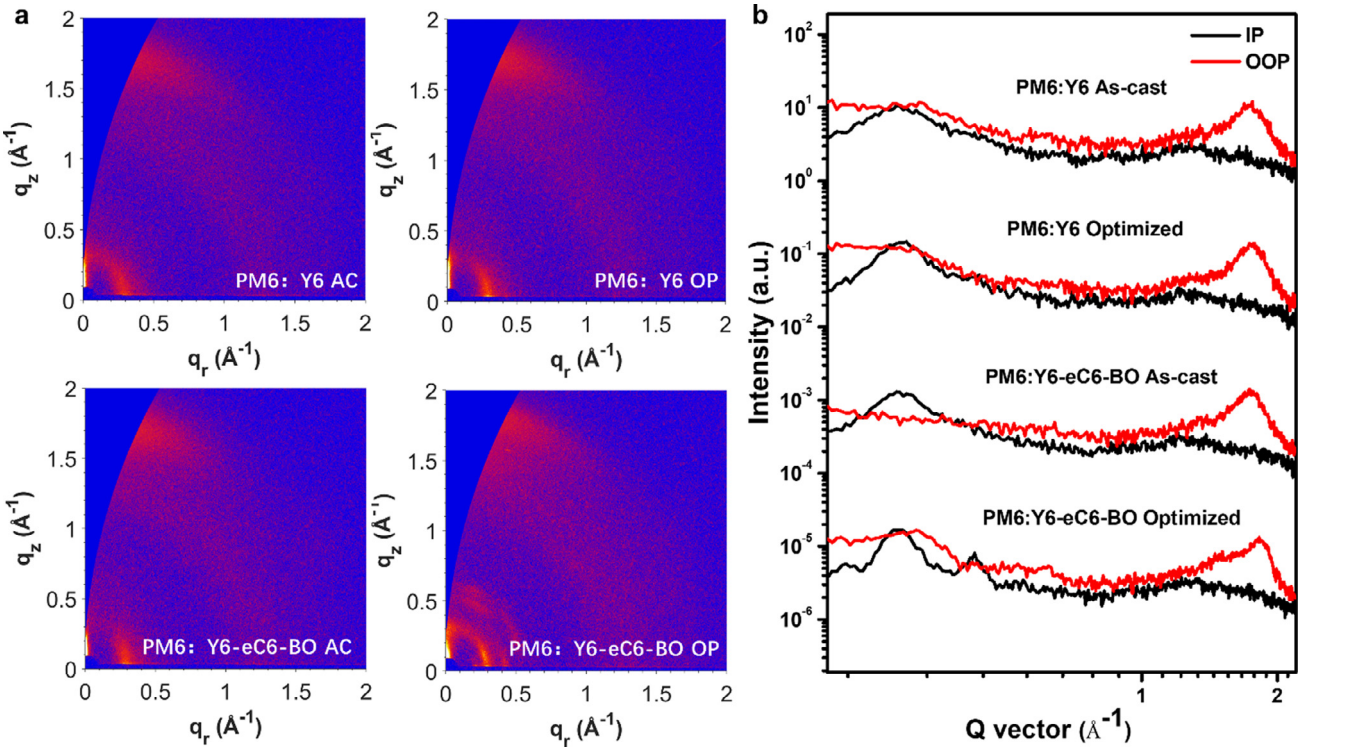

Fig. 4. GIWAXS characterization of the films. (a) Grazing incidence wide-angle X-ray scattering patterns and (b) corresponding profiles of the as-cast (AC) PM6:Y6 film, optimized (OP) PM6:Y6 film, as-cast (AC) PM6:Y6-eC6-BO film and optimized (OP) PM6:Y6-eC6-BO film, respectively.

Table 3
Contact angles and calculated surface energies of PM6, Y6, and Y6-eC6-BO with or with 0.5% CN treatment obtained from the contact angle measurements and the resulting Flory-Huggins interaction parameters of PM6:Y6 and PM6:Y6-eC6-BO blend films.

Material	θ_{Water} a)	θ_{EG} b)	γ(mN/m)	$(\sqrt{\gamma_{PM6}}-\sqrt{\gamma_{NFA}})^2$
PM6	110.475	82.813	24.65	-
Y6	98.244	64.297	37.16	1.28
Y6-eC6-BO	100.163	73.076	26.09	0.02
PM6 (0.5% CN)	105.942	83.453	18.61	-
Y6 (0.5% CN)	103.342	75.921	26.09	0.63
Y6-eC6-BO (0.5% CN)	96.744	71.613	24.46	0.40

a) Water contact angles;
b) Ethylene glycol contact angles

sharply decreased, which suggested that the CN additive played a positive role in improving the miscibility between PM6 and Y6. Interestingly enough, the χ between pristine PM6 and Y6-eC6-BO was the smallest in all studied films, which indicates the excellent miscibility. However, the χ between PM6 and Y6-eC6-BO was increased after being treated with CN, this manifested the miscibility between PM6 and Y6-eC6-BO became inferior after optimization. These results were consistent with the above morphology characterizations and shed light on the morphology evolution of the studied blend film.

To evaluate the influence of the above-mentioned morphology on the charge recombination in the studied devices, the dependence of *J-V* characteristics on light intensity (*P*) was performed [33–35]. In general, the relational expression of J_{sc} versus P can be described as $J_{sc} \propto P^{s}$. When s tends to 1, it suggests that the bimolecular recombination in the devices can be ignored. The dependence of J_{sc} on light intensity for the studied OSCs is plotted in Fig. 5a, the slopes of as-cast PM6:Y6, optimized PM6:Y6, as-cast PM6:Y6-eC6-BO, and optimized PM6:Y6-eC6-BO devices were 0.968, 0.988, 0.998, and 0.995, respectively. Among them, the as-cast PM6:Y6 had a more severe bimolecular recombination that could be responsible for the lowest J_{sc} in all studied OSCs, while the PM6:Y6 OSC exhibited reduced bimolecular recombination after optimization. The biggest slope of 0.998 belonged to as-cast PM6:Y6-eC6-BO OSC, indicating the negligible bimolecular recombination in devices. And the slope of PM6:Y6-eC6-BO OSC was decreased to 0.995 after treatment. Besides, V_{oc} generally follows linear dependence on the natural logarithm of light intensity with a slope of nkT/q, where k is the Boltzmann constant, n is the ideal factor, T is the Kelvin temperature and q is the elementary charge [36]. Generally, the charge recombination is dominated by the bimolecular recombination when the n is close to 1, while the charge recombination is dominated by the trap-assisted recombination or mono-molecular recombination when the n is close to 2. As plotted in Fig. 5b, the slopes of as-cast PM6:Y6, optimized PM6:Y6, as-cast PM6:Y6-eC6-BO, and optimized PM6:Y6-eC6-BO devices were 1.603 kT/q, 1.331 kT/q, 1.267 kT/q, and 1.288 kT/q, respectively. These slopes revealed that the as-cast PM6:Y6 had a more severe trap-assisted recombination or mono-molecular recombination than as-cast PM6:Y6-eC6-BO, and the recombination in the PM6:Y6-based device will be mitigated after optimization while the PM6:Y6-eC6-BO OSC exhibited a reverse trend.

In order to in-depth study the charge generation property of the OSCs, the curves of photocurrent density (J_{ph}) versus effective voltage (V_{eff}) are plotted in Fig. 5c. Here, $J_{ph}$is expressed as $J_{ph} = J_L - J_D$, where J_L and J_D are the photocurrent density under illumination and in the dark, respectively. V_{eff} is defined as $V_{eff} = V_0 - V_a$, where V_0 is the voltage where J_{ph}equals zero and $V_a$is applied bias voltage [37]. In general, all photogenerated excitons could be dissociated into free charges at high V_{eff}(in this case, 2 V). Thus, the charge dissociation possibility P(E,T) could be extracted from J_{ph}/J_{sat}. As shown in Fig. 5c, the P(E,T) values of as-cast PM6:Y6, optimized PM6:Y6, as-cast PM6:Y6-eC6-BO, and optimized PM6:Y6-eC6-BO devices were 0.957, 0.969, 0.988, and 0.978, respectively. The P(E,T) of PM6:Y6 OSC was increased after optimization, which may be ascribed to the increased D/A interfaces that facilitated the charge dissociation. Besides, the as-cast PM6:Y6-eC6-BO afforded the highest value of 0.998 due to the fact that the suitable phase separation of donor and acceptor gave rise to increased D/A interfaces which were verified by morphology images. In addition, the charge transfer in

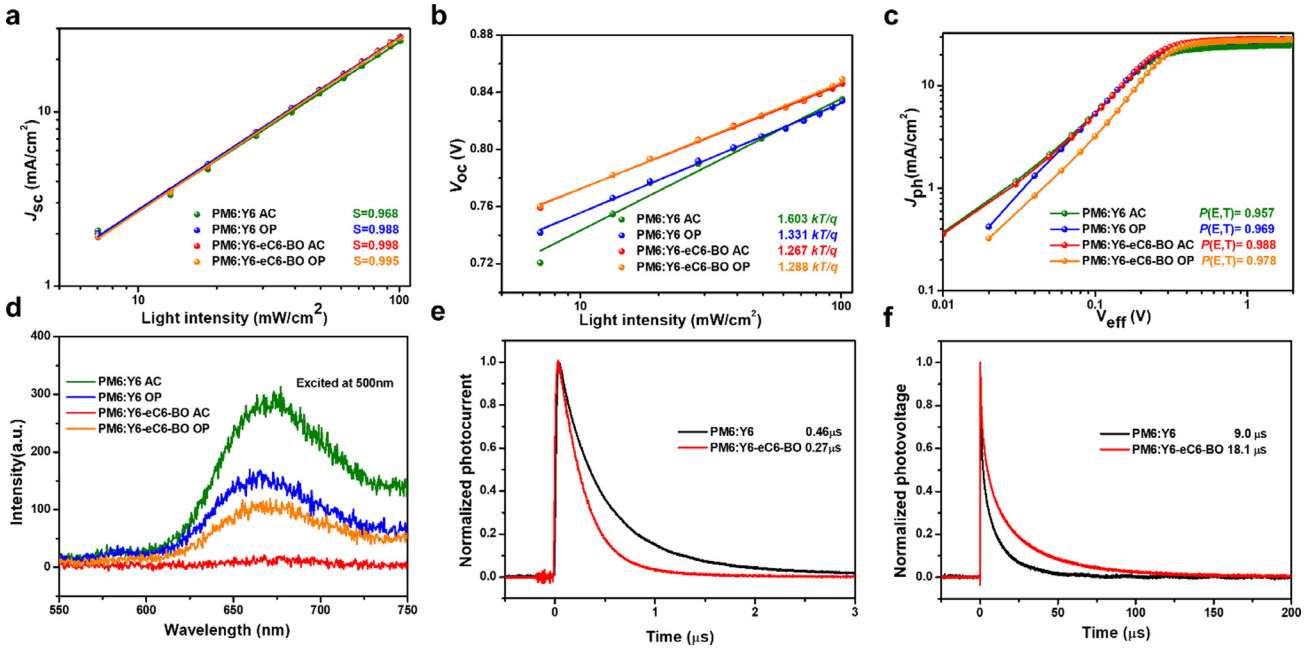

Fig. 5. Charge recombination and extraction characteristics of the OSCs. Light intensity dependence of (a) J_{sc} and (b) V_{oc} of as-cast PM6:Y6, optimized PM6:Y6, as-cast PM6:Y6-eC6-BO and optimized PM6:Y6-eC6-BO devices. (c) Photocurrent density (J_{ph}) versus effective voltage (V_{eff}) characteristics and (d) PL of as-cast PM6:Y6, optimized PM6:Y6, as-cast PM6:Y6-eC6-BO and optimized PM6:Y6-eC6-BO blend films (e) Transient photocurrent and (f) Transient photovoltage of as-cast PM6:Y6 and PM6:Y6-eC6-BO devices.

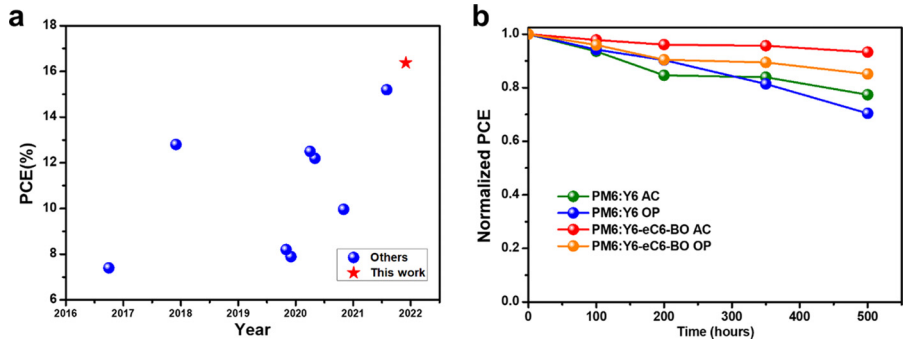

Fig. 6. The comparison of this work with the reported results and the device stability characterization of different OSCs. (a) Summary of the reported as-cast OSCs processed from non-halogen solvents in recent years. (b) The long-term stability test of the studied devices stored in the N_2 atmosphere.

Table 4
Photovoltaic parameters of the as-cast OSCs processed from *o*-XY under 1 sun illumination.

BHJ	V_{oc} (V)	J_{sc}(mA cm^{-2})	FF (%)	PCE (%)
PM6:Y6	0.775	18.45	63.08	9.02
PM6:Y6-eC6-BO	0.844	25.72	75.47	16.38

the blend film can be studied by steady-state photoluminescence (PL) quenching [38]. As illustrated in Fig. 5d, the excitation wavelength is 500 nm. The PL intensity of the studied blend films was lower than the pristine PM6 film (as shown in Fig. S7), this can be attributed to charge transfer in blend films. A decrease in PL intensity of PM6:Y6 film after optimization showed an improved charge transfer from donor to NFA acceptor due to the enlargement of the D/A interface area. And the increase in PL intensity of PM6: Y6-eC6-BO film after treated with CN and thermal annealing could be attributed to the reduced D/A interfaces as well.

We carried out transient photocurrent (TPC) and transient photovoltage (TPV) measurements to investigate the charge extraction and recombination properties of the as-cast OSCs, respectively [39]. As plotted in Fig. 5e, the as-cast PM6:Y6 OSC showed a longer charge extraction time of 0.46 μs than the as-cast PM6: Y6-eC6-BO OSC (0.27 μs). And the over-large phase separation of PM6 and Y6 should be responsible for this result. Meanwhile, as shown in Fig. 5d, the extracted carrier lifetimes of as-cast PM6:Y6 and PM6: Y6-eC6-BO were 9.0 μs and 18.1 μs, respectively. This result indicated that charge recombination will more readily occur in Y6-based devices. Besides, the carrier transport property of as-cast PM6:Y6, optimized PM6:Y6, as-cast PM6:Y6-eC6-BO, and optimized PM6:Y6-eC6-BO devices was investigated by the space charge limited current (SCLC) method [40,41]. The extracted hole and electron mobilities were plotted in Fig. S8, among them, the as-cast PM6:Y6 possessed a low μ_h of 7.2×10^{-5} cm^2 V^{-1}s^{-1} and μ_e of 6.15×10^{-5} cm^2 V^{-1}s^{-1}, while the as-cast PM6:Y6-eC6-BO device afforded a high μ_h of 4.55×10^{-4} cm^2 V^{-1}s^{-1} and μ_e of 4.54×10^{-4} cm^2 V^{-1}s^{-1} and balanced μ_h/μ_e, resulting in a higher FF than other devices. Higher electron mobility of PM6:Y6-eC6-BO device was attained after treatment owing to the stronger crystallization.

Although a high PCE of over 17% was obtained, however, these as-cast devices were processed from chloroform (CF) solvent. Compared with non-halogen solvents, CF has some drawbacks that prevent the large-scale production of OSCs in the future, such as toxic, volatile, expensive [42–44]. Therefore, we positively choose ortho-xylene (*o*-XY) with a high-boiling point as the processing solvent. As summarized in Table 4 (the original *J*-*V* curves are plotted in Fig. S9), the as-cast PM6:Y6 processed from *o*-XY only exhibited a poor PCE of 9.02%, which is consistent with the previous result. Nevertheless, the as-cast OSC based on PM6: Y6-eC6-BO processed from *o*-XY showed a comparable PCE of 16.38% in contrast with CF processing solvent. To our best knowledge, this is the highest PCE for the as-cast non-halogenated processed OSCs up to now (as shown in Fig. 6a). Moreover, the stability test of relevant devices was performed as well, the relationship of normalized PCE versus aging time was plotted in Fig. 6b. The Y6-eC6-BO-based devices showed better stability than the Y6-based counterpart, which could be attributed to a bigger χ between PM6 and Y6 than that between PM6 and Y6-eC6-BO thus will result in over-large phase separation [45,46]. Among them, the as-cast PM6: Y6-eC6-BO OSC displayed better stability than others and maintained about 93.2% of its original PCE after aging of 500 hours. Also, the rapid degradation of the CN-additive treated PM6: Y6-eC6-BO OSC may be that the residual CN additive played an adverse role in morphology. The optimized PM6:Y6 OSC only retained 70.4% of its initial PCE after aging of 500 hours. This result indicates that the as-cast OSCs have a great potential for commercialization in the future.

3. Conclusion

To conclude, we synthesized a new A-DA′D-A type acceptor, Y6-eC6-BO, by shortening the straight alkyl side-chains on the thiophene position from C_{11} to C_6 as well as lengthening the branched alkyl side-chains on the pyrrole position of Y6. The Y6-eC6-BO maintained a favorable crystalline ability and miscibility simultaneously. The better morphology features improved the charge dissociation, charge transport and suppressed the charge recombination in the Y6-eC6-BO-based devices. The strong crystallinity of Y6-eC6-BO enabled high-performance OSC of over 17% efficiency without the treatments of additive and thermal annealing. Also, a PCE of 16.38% was achieved in the ortho-xylene (*o*-XY) processed as-cast PM6: Y6-eC6-BO OSCs, which was listed among the highest values reported in the non-halogenated-solvent processed as-cast OSCs to date. In addition, the as-cast PM6: Y6-eC6-BO OSCs showed better stability than the treated counterpart devices. These results not only demonstrate high-performance as-cast PM6: Y6-eC6-BO OSCs which has a great potential in practical applications in the future, but also manifest that tailoring the alkyl side chains on Y6 is a feasible and simple approach to achieve high-performance as-cast OSCs.

Declaration of competing interest

The authors declare that they have no conflicts of interest in this work.

Acknowledgments

Y. Zou acknowledges the National Natural Science Foundation of China (21875286 and 52125306), the National Key Research and De-

velopment Program of China (2017YFA0206600). X. Lu acknowledges the Research Grants Council of Hong Kong (14303519).

Supplementary materials

Supplementary material associated with this article can be found, in the online version, at doi:10.1016/j.fmre.2022.01.025.

References

[1] J. Hou, O. Inganäs, R.H. Friend, et al., Organic solar cells based on non-fullerene acceptors, Nat. Mater. 17 (2) (2018) 119–128.
[2] G. Li, R. Zhu, Y. Yang, Polymer solar cells, Nat. Photonics 6 (2012) 153.
[3] P. Cheng, G. Li, X. Zhan, et al., Next-generation organic photovoltaics based on non-fullerene acceptors, Nat Photonics 12 (3) (2018) 131–142.
[4] L. Feng, J. Yuan, Z. Zhang, et al., Thieno [3,2-b]pyrrolo-Fused Pentacyclic Benzotriazole-Based Acceptor for Efficient Organic Photovoltaics, ACS Appl. Mater. Interfaces 9 (37) (2017) 31985–31992.
[5] J. Yuan, Y. Zhang, L. Zhou, et al., Single-junction organic solar cell with over 15% efficiency using fused-ring acceptor with electron-deficient core, Joule 3 (4) (2019) 1140–1151.
[6] G. Zhang, X.-K. Chen, J. Xiao, et al., Delocalization of exciton and electron wavefunction in non-fullerene acceptor molecules enables efficient organic solar cells, Nat. Commun. 11 (1) (2020) 1–10.
[7] C. Li, J. Zhou, J. Song, et al., Non-fullerene acceptors with branched side chains and improved molecular packing to exceed 18% efficiency in organic solar cells, Nature Energy 6 (6) (2021) 605–613.
[8] M. Zhang, L. Zhu, G. Zhou, et al., Single-layered organic photovoltaics with double cascading charge transport pathways: 18% efficiencies, Nat. Commun. 12 (1) (2021) 309.
[9] J. Wang, Z. Zheng, Y. Zu, et al., A tandem organic photovoltaic cell with 19.6% efficiency enabled by light distribution control, Adv. Mater. 33 (39) (2021) 2102787.
[10] P. Bi, S. Zhang, Z. Chen, et al., Reduced non-radiative charge recombination enables organic photovoltaic cell approaching 19% efficiency, Joule 5 (9) (2021) 2408–2419.
[11] Y. Cui, H. Yao, J. Zhang, et al., Single-Junction Organic Photovoltaic Cells with Approaching 18% Efficiency, Adv. Mater. 32 (19) (2020) 1908205.
[12] Y. Kim, S.A. Choulis, J. Nelson, et al., Device annealing effect in organic solar cells with blends of regioregular poly(3-hexylthiophene) and soluble fullerene, Appl. Phys. Lett. 86 (6) (2005) 063502.
[13] J. Song, L. Zhu, C. Li, et al., High-efficiency organic solar cells with low voltage loss induced by solvent additive strategy, Matter 4 (7) (2021) 2542–2552.
[14] J. Lv, H. Tang, J. Huang, et al., Additive-induced miscibility regulation and hierarchical morphology enable 17.5% binary organic solar cells, Energy Environ. Sci. 14 (5) (2021) 3044–3052.
[15] J. Ge, L. Hong, W. Song, et al., Solvent Annealing Enables 15.39% Efficiency All-Small-Molecule Solar Cells through Improved Molecule Interconnection and Reduced Non-Radiative Loss, Adv. Energy Mater. 11 (22) (2021) 2100800.
[16] M. Jiang, H.-r. Bai, H.-f. Zhi, et al., Two-Pronged Effect of Warm Solution and Solvent-Vapor Annealing for Efficient and Stable All-Small-Molecule Organic Solar Cells, ACS Energy Letters 6 (8) (2021) 2898–2906.
[17] S.J. Lou, J.M. Szarko, T. Xu, et al., Effects of additives on the morphology of solution phase aggregates formed by active layer components of high-efficiency organic solar cells, J. Am. Chem. Soc. 133 (51) (2011) 20661–20663.
[18] X. Xu, D. Li, J. Yuan, et al., Recent advances in stability of organic solar cells, EnergyChem 3 (1) (2021) 100046.
[19] B.J. Tremolet de Villers, K.A. O'Hara, D.P. Ostrowski, et al., Removal of Residual Diiodooctane Improves Photostability of High-Performance Organic Solar Cell Polymers, Chem Mater 28 (3) (2016) 876–884.
[20] X. Xu, J. Xiao, G. Zhang, et al., Interface-enhanced organic solar cells with extrapolated T80 lifetimes of over 20 years, Science Bulletin 65 (3) (2020) 208–216.
[21] A. Classen, T. Heumueller, I. Wabra, et al., Revealing Hidden UV Instabilities in Organic Solar Cells by Correlating Device and Material Stability, Adv. Energy Mater. 9 (39) (2019) 1902124.
[22] R. Ma, Y. Tao, Y. Chen, et al., Achieving 16.68% efficiency ternary as-cast organic solar cells, Science China Chemistry 64 (4) (2021) 581–589.
[23] H. Feng, X. Song, Z. Zhang, et al., Molecular Orientation Unified Nonfullerene Acceptor Enabling 14% Efficiency As-Cast Organic Solar Cells, Adv. Funct. Mater. 29 (36) (2019) 1903269.
[24] X. Chen, B. Kan, Y. Kan, et al., As-Cast Ternary Organic Solar Cells Based on an Asymmetric Side-Chains Featured Acceptor with Reduced Voltage Loss and 14.0% Efficiency, Adv. Funct. Mater. 30 (11) (2020) 1909535.
[25] Z. Zhang, Y. Li, G. Cai, et al., Selenium heterocyclic electron acceptor with small urbach energy for as-cast high-performance organic solar cells, J. Am. Chem. Soc. 142 (44) (2020) 18741–18745.
[26] T. Li, K. Wang, G. Cai, et al., Asymmetric Glycolated Substitution for Enhanced Permittivity and Ecocompatibility of High-Performance Photovoltaic Electron Acceptor, JACS Au (2021).
[27] K. Wang, W. Li, X. Guo, et al., Optimizing the Alkyl Side-Chain Design of a Wide Band-Gap Polymer Donor for Attaining Nonfullerene Organic Solar Cells with High Efficiency Using a Nonhalogenated Solvent, Chem. Mater. 33 (15) (2021) 5981–5990.
[28] P. Müller-Buschbaum, The active layer morphology of organic solar cells probed with grazing incidence scattering techniques, Adv. Mater. 26 (46) (2014) 7692–7709.
[29] F. Zhao, C. Wang, X. Zhan, Morphology control in organic solar cells, Adv. Energy Mater. 8 (28) (2018) 1703147.
[30] T.L. Benanti, D. Venkataraman, Organic solar cells: An overview focusing on active layer morphology, Photosynth. Res. 87 (1) (2006) 73–81.
[31] S. Nilsson, A. Bernasik, A. Budkowski, et al., Morphology and phase segregation of spin-casted films of polyfluorene/PCBM blends, Macromolecules 40 (23) (2007) 8291–8301.
[32] D.K. Owens, R. Wendt, Estimation of the surface free energy of polymers, J. Appl. Polym. Sci. 13 (8) (1969) 1741–1747.
[33] L.J.A. Koster, M. Kemerink, M.M. Wienk, et al., Quantifying bimolecular recombination losses in organic bulk heterojunction solar cells, Adv. Mater. 23 (14) (2011) 1670–1674.
[34] L.J.A. Koster, V.D. Mihailetchi, R. Ramaker, et al., Light intensity dependence of open-circuit voltage of polymer: fullerene solar cells, Appl. Phys. Lett. 86 (12) (2005) 123509.
[35] L.J.A. Koster, V. Mihailetchi, H. Xie, et al., Origin of the light intensity dependence of the short-circuit current of polymer/fullerene solar cells, Appl. Phys. Lett. 87 (20) (2005) 203502.
[36] N.K. Elumalai, A. Uddin, Open circuit voltage of organic solar cells: an in-depth review, Energy Environ. Sci. 9 (2) (2016) 391–410.
[37] L. Lu, T. Xu, W. Chen, et al., Ternary blend polymer solar cells with enhanced power conversion efficiency, Nat. Photonics 8 (9) (2014) 716–722.
[38] K. Tvingstedt, K. Vandewal, F. Zhang, et al., On the dissociation efficiency of charge transfer excitons and frenkel excitons in organic solar cells: a luminescence quenching study, J. Phys. Chem. C 114 (49) (2010) 21824–21832.
[39] Z. Li, F. Gao, N.C. Greenham, et al., Comparison of the Operation of Polymer/Fullerene, Polymer/Polymer, and Polymer/Nanocrystal Solar Cells: A Transient Photocurrent and Photovoltage Study, Adv. Funct. Mater. 21 (8) (2011) 1419–1431.
[40] V. Mihailetchi, J. Wildeman, P. Blom, Space-charge limited photocurrent, Phys. Rev. Lett. 94 (12) (2005) 126602.
[41] P. Murgatroyd, Theory of space-charge-limited current enhanced by Frenkel effect, J. Phys. D Appl. Phys. 3 (2) (1970) 151.
[42] S. Zhang, L. Ye, H. Zhang, et al., Green-solvent-processable organic solar cells, Mater. Today 19 (9) (2016) 533–543.
[43] X. Chen, X. Liu, M.A. Burgers, et al., Green-Solvent-Processed Molecular Solar Cells, Angew. Chem. 126 (52) (2014) 14606–14609.
[44] J. Zhao, Y. Li, G. Yang, et al., Efficient organic solar cells processed from hydrocarbon solvents, Nature Energy 1 (2) (2016) 1–7.
[45] J.D.o. Perea, S. Langner, M. Salvador, et al., Introducing a new potential figure of merit for evaluating microstructure stability in photovoltaic polymer-fullerene blends, J. Phys. Chem. C 121 (33) (2017) 18153–18161.
[46] J. Xiao, M. Ren, G. Zhang, et al., An Operando Study on the Photostability of Nonfullerene Organic Solar Cells, Solar RRL 3 (7) (2019) 1900077.

Xiang Xu received his bachelor degree in Nanchang University, M.S. degree in South China University of Technology (SCUT), and is currently a Ph.D. student at college of Chemistry and Chemical Engineering, Central South University (CSU), where he is a member of the Yingping Zou research group. His research interests mainly focus on organic solar cells.

Yingping Zou received her Ph. D. degree from Institute of Chemistry, Chinese Academy of Sciences (ICCAS) in 2008, then in the following years she performed her postdoctoral/visiting research in Laval University and in Stanford University. She was promoted to full professor in 2014 in Central South University. Currently her researches focus on the organic small molecules/polymers for high performance optoelectronic devices. She has published more than 200 peer-review papers with over 12,800 citations and H index is 51.